Temperature-dependent phonon Raman scattering and spectroscopic ellipsometry of pure and Ca-doped $Sr_x Ba_{1-x} Nb_2O_6$ ferroelectric ceramics across the phase transition region

2016 J. Phys. D: Appl. Phys. 49 035307

(http://iopscience.iop.org/0022-3727/49/3/035307)

IOP Publishing Journal of Physics D: Applied Physics

J. Phys. D: Appl. Phys. **49** (2016) 035307 (9pp) doi:10.1088/0022-3727/49/3/035307

Temperature-dependent phonon Raman scattering and spectroscopic ellipsometry of pure and Ca-doped $Sr_xBa_{1-x}Nb_2O_6$ ferroelectric ceramics across the phase transition region

Liang Peng[1], Kai Jiang[1], Jinzhong Zhang[1], Zhigao Hu[1], Genshui Wang[2], Xianlin Dong[2] and Junhao Chu[1]

[1] Department of Electronic Engineering, East China Normal University, Shanghai 200241, People's Republic of China

[2] Key Laboratory of Inorganic Functional Materials and Devices, Shanghai Institute of Ceramics, Chinese Academy of Sciences, Shanghai 200050, People's Republic of China

E-mail: zghu@ee.ecnu.edu.cn

Received 17 July 2015, revised 23 November 2015
Accepted for publication 25 November 2015
Published 22 December 2015

Abstract

Optical phonons and the phase transition of relaxor ferroelectric ceramics $Sr_xBa_{1-x}Nb_2O_6$ (SBN) and $Ca_y(Sr_{0.5}Ba_{0.5})_{1-y}Nb_2O_6$ (CSBN) with different composition ($0.3 \leqslant x \leqslant 0.5$, $0.1 \leqslant y \leqslant 0.2$) have been investigated by variable-temperature Raman scattering and spectroscopic ellipsometry. The anomalous temperature dependence of Tauc gap energy (E_t) is used to fit the phonon energy dependence of the permittivity, and the Raman intensity of some interesting optical phonons can be ascribed to the phase transition from a ferroelectric to a paraelectric structure. The Curie temperature of SBN decreases from 556 to 359 K with increasing Sr composition, which can be attributed to the substitution of smaller Sr^{2+} for Ba^{2+}. On increasing the Ca composition, however, the phase transition temperature of CSBN remains nearly unchanged at about 350 K. This could be due to the fact that most doped Ca^{2+} ions move into the oxygen ion site and exhibit no obvious effect on the vibrational properties. Therefore, the general disorder which results from Sr^{2+} substituting Ba^{2+}, dominates the phase transition process for SBN-based ferroelectric oxides. Meanwhile, the dielectric functions from 200 to 600 K have been evaluated with the aid of the Tauc–Lorentz model. The electronic transition is located at about 5 eV and decreases with increasing temperature for all the samples. Moreover, the phase transition temperature range derived from the spectroscopic ellipsometry agrees well with that from the Raman scattering. It reveals that the variation of the fundamental energy gap may be associated with the phase transition of SBN ceramics. Both Raman scattering and spectroscopic ellipsometry are proven to be a effective method of exploring the phase transition of ferroelectric oxides.

Keywords: relaxor ferroelectrics, phase transition, Tauc gap

(Some figures may appear in colour only in the online journal)

1. Introduction

Disordered ferroelectric systems are of great interest from the fundamental as well as application points of view. One important class of such disordered systems consists of relaxor ferroelectrics, such as lead-based $Pb(Mg_{1/3}Nb_{2/3})O_3$-$xPbTiO_3$, $PbSc_{1/2}Ta_{1/2}O_3$, Pb-free $Bi_xNa_{1-x}TiO_3$, $K_{1-x}Na_xNbO_3$ and $Sr_xBa_{1-x}Nb_2O_6$ (SBN) [1–7]. Among them, the uniaxial relaxor ferroelectric SBN is of particular interest due to its well-known pyroelectric, electro-optic, photorefractive, piezoelectric and non-linear optical properties [8, 9]. It has various potential applications such as pyroelectric infrared detection, holographic data storage, phase conjugation and the generation of photorefractive solitons [10–14]. The SBN crystal was first studied by Glass *et al* in 1968 as a fast and sensitive detector of infrared radiation, and some studies have been performed on ferroelectric SBN ever since [15–18]. The structure of ferroelectric tungsten bronze-type $Sr_{0.27}Ba_{0.75}Nb_2O_{5.78}$ crystal was reported by Jamieson *et al* in 1968 [19]. It was reported that a different Sr/Ba ratio can lead to a varying distortion of the NbO_6 octahedron, which leads to changes in the different dielectric and pyroelectric properties [18, 20].

Several methods can be used to probe the phase transition of ferroelectric materials such as dielectric measurement, second harmonic generation and light scattering. Raman scattering is one of the most powerful non-destructive techniques to investigate structural phase transitions. It was found that increasing the Sr content can lead to a decrease in the Curie temperature (T_c) for SBN materials using dielectric spectroscopy measurement [16, 22]. Structural changes corresponding to the crystal symmetry have a significant effect on the Raman spectrum [23, 24]. In particular, the optical modes, which are associated with the ferroelectric to paraelectric phase transition, are of great interest. Speghini *et al* investigated the changes of the main Raman peak at about 630 cm^{-1} with the temperature and found T_c varies almost linearly with increasing the Sr content ($x = 0.33$, 0.50 and 0.61) [25]. Several dopants have been introduced to modify the dielectric and pyroelectric properties of SBN, such as Cr, K, Na and rare earth. Yao *et al* revealed that the piezoelectric and pyroelectric performances of $(Sr_{0.6}Ba_{0.4})_4Na_2Nb_{10}O_{30}$ ceramics were enhanced by Ca doping [26]. Importantly, Zhang *et al* found that the dielectric, ferroelectric and pyroelectric properties of $Ca_y(Sr_{0.5}Ba_{0.5})_{1-y}Nb_2O_6$ (CSBN) vary significantly with different Ca fractions [27]. The pyroelectric properties of CSBN could be enhanced remarkably due to Ca addition and reach the maximum values at $y = 0.15$. Unfortunately, there are few studies about the effects of the Sr/Ba ratio on the vibrational modes for SBN ceramics, and the effects of Ca doping on the phase transition temperature of SBN have not been reported yet. In this article, we study how optical properties change with the doping of Ca in SBN.

As we know, a material's optical properties like the dispersion of the refractive index and optical band gap energy are of significant value in the design and optimisation of optical devices. Knowledge about these properties is helpful for understanding phase transformation in SBN, especially for an explanation of the relaxor property of the ceramics. The refractive index of SBN was first reported by Venturini *et al* in the wavelength range from 425 to 1600 nm in 1968 [28]. Studies about the dispersion of the refractive index of SBN have been carried out ever since [29, 30]. On the contrary, the optical band gap has not been investigated sufficiently so far. Thus, information about the near band gap electronic transition, especially the correlation between phase transformation and temperature dependence energy band structure variation is not available. It is essential for us to apply spectroscopic ellipsometry (SE) measurements to investigate the band gap energy and other significant optical properties of SBN and CSBN ceramics in a wide composition and temperature range. SE is regarded as a sensitive measurement method to characterise the dielectric functions of condensed matter materials. Note that most of these studies have been limited to single crystals [17, 21, 25, 31]. However, ceramics could be more widely used owing to their low cost and easy fabrication. Furthermore, few reports about complex dielectric functions of SBN ceramics have been presented up to now.

The purpose of this paper is to investigate the lattice vibration and electronic properties of $Ca_y(Sr_xBa_{1-x})_{1-y}Nb_2O_6$ ceramics with different Sr/Ba ratios and different Ca dopants by temperature-dependent Raman spectroscopy and SE experiment. The phase transition from ferroelectric to paraelectric can be detected from the main mode variation with temperature. Moreover, the relationship between the energy band gap and phase transition of SBN ceramics is discussed in detail.

2. Experimental details

The SBN ($Sr_xBa_{1-x}Nb_2O_6$, $x = 0.3$, 0.4, and 0.5) and CSBN ($Ca_y(Sr_{0.5}Ba_{0.5})_{1-y}Nb_2O_6$, $y = 0.1$, 0.15, and 0.2) ceramics were prepared by a traditional solid-state ceramic fabrication method. $SrCO_3$ (99%), $BaCO_3$ (99%), $CaCO_3$ (99%) and Nb_2O_5 (99%) were used as starting materials. Details of the fabrication process of the ceramic can be found elsewhere [22, 27]. It is noted that the CSBN ceramics with different Ca composition are fabricated on the basis of SBN ($x = 0.5$). All the SBN and CSBN ceramic wafers were double-side polished with a mechanical polishing process to smooth the surface. This process consists of three procedures: coarse grinding, fine grinding and polishing. Then, the ceramics were rigorously cleaned in pure ethanol with an ultrasonic bath and rinsed several times with deionised water for spectral measurements.

The x-ray diffraction (XRD) patterns indicate that SBN and CSBN ceramics were both crystallised into a pure tetragonal tungsten bronze structure, while no second phase was detected at room temperature (RT) [22, 27]. The Raman scattering experiments were carried out using a Jobin–Yvon LabRAM HR 800 UV micro-Raman spectrometer. A laser with a wavelength of 632.8 nm was used as the excitation source and an air-cooled charge coupled device (CCD) was used to collect the scattered signal dispersed on 1800 grooves mm^{-1} grating in the frequency range of 10–1000 cm^{-1}, with the use of an ultra low frequency (ULF) filter. The spectral resolution of the Raman spectra is better than 0.65 cm^{-1}. Temperature-dependent Raman measurements from 150 to 750 K were performed using a Linkam THMSE 600 heating

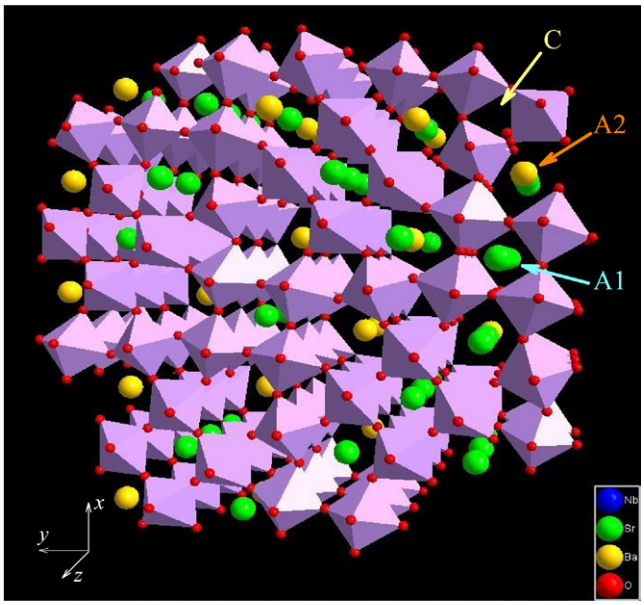

Figure 1. Crystal structure for SBN ceramics, which shows the connectivity of the NbO_6 octahedra. A_1-site: Sr, A_2-site: Sr or Ba and *C*-site: vacant site.

stage and the set-point stability is better than 0.5 K. The temperature-dependent SE experiments were carried out in the photon energy range of 1.5–6.0 eV by a vertical variable-angle near-infrared ultraviolet SE (V-VASE by Woollam Co, Inc). It was measured with a zone average polariser at an incident angle of 70° and the spectral interval was set to two nm. For the variable-temperature measurements, the samples were mounted onto an Instec cell and the temperature could be controlled from 200 to 600 K with a precision of about ±1 K. The system was continuously purged with dry N_2 not only to protect the sample surface from contamination but also to avoid water vapour in the ambient. Note that the window corrections were included as a part of the model during the fitting analysis.

3. Results and discussions

Let us first briefly comment on the main features of the structure and Raman spectrum of SBN. At the ambient temperature and pressure, the ferroelectric phase of SBN belongs to the point group C_{4v} with space group *P*4 *bm* and five formula units per unit cell [19]. This is a tetragonal tungsten bronze (TTB)-type disordered structure, and consists of a framework of NbO_6 octahedra sharing the corner oxygen to form three different size cavities with the unit cell formula $(A1)_2(A2)_4C_4(B1)_2(B2)_8O_{30}$. For SBN oxide, different cations occupy both the A1 and A2 symmetry sites, forming a partially filled TTB structure. The tungsten bronze crystal structure of ferroelectric SBN is illustrated in figure 1. The A1 symmetry sites (12-fold correlated site inside the squared channels) are partially occupied by Sr^{2+} ions. While the A2 symmetry sites (15-fold correlated site inside the pentagonal ones) are randomly occupied by Sr^{2+} and Ba^{2+} ions. Moreover, the C site occupies a small tricapped trigonal prism of oxygen atoms and it is partly distorted. The B sites are completely filled by Nb^{5+} ions [19, 21]. The ferroelectric to paraelectric phase transition is accompanied by a structural phase change from tetragonal system with point group C_{4v} to D_{2d} point group symmetry. For the *P*4*bm* space group there are 138 possible vibrational normal modes and they can be classified according to the following irreducible representations: $\Gamma_{vib} = 19A_1(z) + 15A_2 + 14B_1 + 18B_2 + 36E(x) + 36E(y)$, where x, y and z indicate the polarisation direction of the IR active modes (z being the ferroelectric axis) [25]. Three of these modes (belonging to A_1, $E(x)$ and $E(y)$ representations) are acoustic modes. The other modes, except for the A_2 modes, are Raman active. Therefore, there are 120 Raman active modes. However, the number of modes observed experimentally is significantly less due to the weak strength and the possible overlapping of the same symmetry vibration. The ferroelectric to paraelectric phase transition of SBN is considered to be due to the metal atoms moving back into the oxygen planes in NbO_6 octahedra [18, 32, 33]. The internal vibrational modes of these octahedra are of interest for investigation.

Figures 2(a) and (b) show the fitting of the Raman spectra of the SBN ceramics recorded at 150 K and 600 K, respectively. The peak position of each component, i.e. the natural frequency of each Raman active mode was obtained by fitting the experimental spectra and devolution of the fitted curves into individual Lorentzian components. In the fitting process, Raman spectra were corrected for the Bose–Einstein temperature factor to eliminate the contribution of the Bose–Einstein population factor from the measured Raman intensity. The reduced Raman intensity is written as $R(\nu) = I(\nu)/[n(\nu) + 1]$, where $I(\nu)$ corresponds to the measured Raman intensity and $n(\nu) = [e^{h\nu/kT} - 1]^{-1}$ is the Bose–Einstein factor [14]. A Lorentz oscillator model is adopted for the fitting of the Raman spectra. The best fitting of the Raman spectra for all the samples is presented in figure 2(c). According to the vibrational modes of NbO_6 octahedra, the phonons including V_1 (103 cm^{-1}), V_2 (254 cm^{-1}), V_3 (608 and 640 cm^{-1}) and V_4 (851 cm^{-1}) can be found [34]. The very strong bands V_1 and weak band V_4 are attributed to the O–Nb–O bending vibration modes. The V_3 modes, which are in fact a combination of two optical phonons corresponding to a stretch type vibration of the NbO_6 octahedra, decrease with increasing the Sr/Ba ratio [34]. For SBN, the frequencies of the two V_3 modes decrease from 647 and 615 cm^{-1}–640 and 610 cm^{-1}, respectively (see figures 2(d) and (e) that show the two-phonon frequency shift of the CSBN ceramics). On increasing the Ca content, the frequencies of the phonons show the same trend, decreasing from 640 and 610 cm^{-1}–633 and 596 cm^{-1}.

A systematic investigation of the temperature evolution of the phonon modes is necessary for the SBN and CSBN ceramics. Figure 3 presents the Raman spectra for the SBN ($x = 0.5$) and CSBN ($y = 0.15$) ceramics in the temperature range from 150 to 750 K. It should be pointed out that the presence of strong lattice disorder gives rise to significant broadening of the bands and allows the observation of a limited number of spectral features. The weak band (850 cm^{-1}), which is related to the silent mode V_4, was detected in the Raman spectra. This mode is less sensitive to temperature

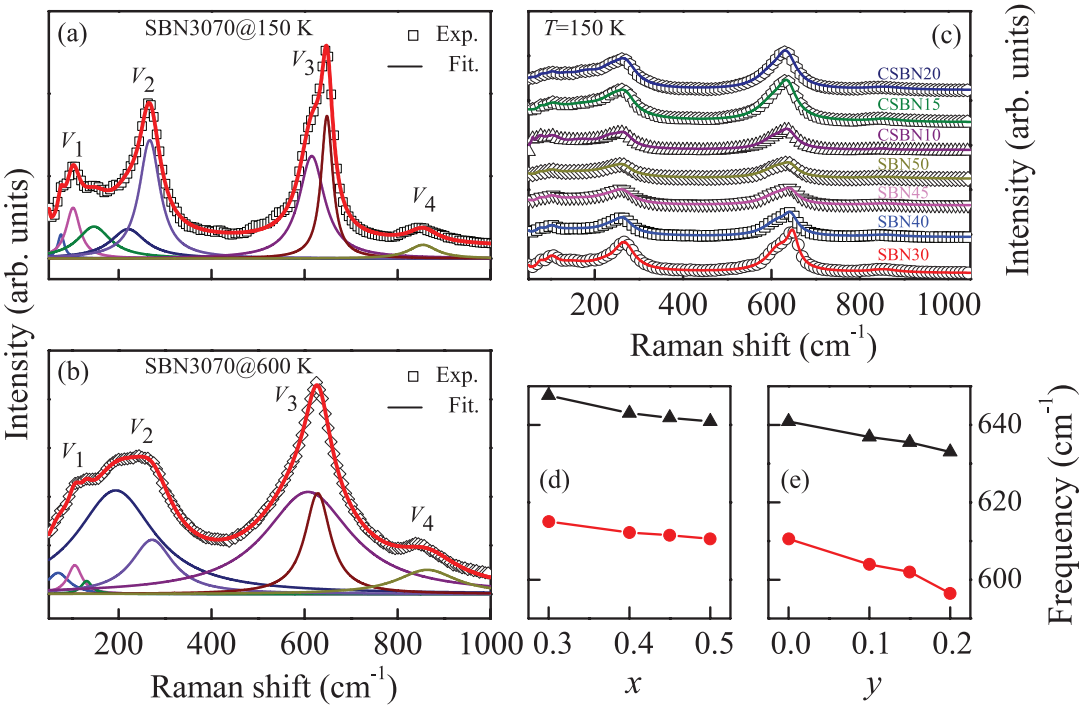

Figure 2. Raman spectra of the SBN ceramics with different Sr composition and CSBN ceramics with different Ca composition at (a) 150 K and (b) 300 K. (c) Experimental Raman spectrum (dotted lines) and Lorentzian fitting results (solid lines) of the $Sr_{0.3}Ba_{0.7}Nb_2O_6$ ceramics at 150 K (d) and (e) the two frequencies of the V_3 modes located at about 610 and 640 cm^{-1} as a function of the Sr and Ca composition, respectively.

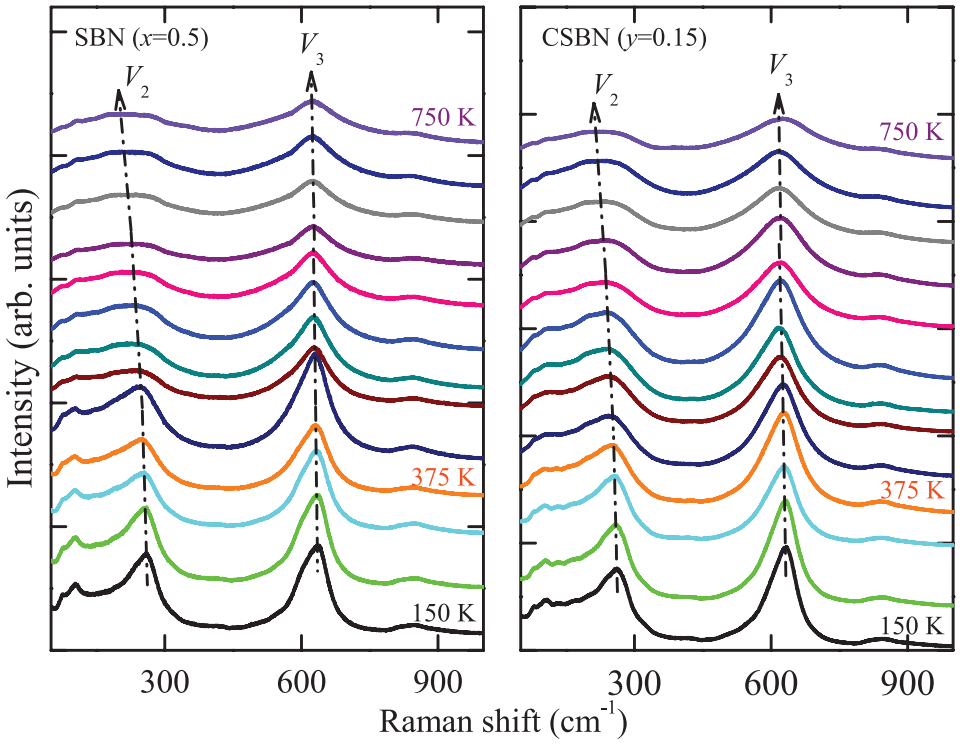

Figure 3. Temperature dependence of Raman spectra for SBN ceramics with the composition of $x = 0.5$ and CSBN ceramics with a Ca composition of $y = 0.15$. The dashed line arrows are applied as a guide for the eyes.

changes during the phase transition because it contributes little to the polarisation [25]. The V_3 phonons are polarised along the z axis, along which the atoms must be displaced during the phase transition. Therefore, we concentrate on the variation of the V_3 modes to investigate the phase transition of SBN. Meanwhile, the V_2 (254 cm^{-1}) phonon mode is shifted toward a lower frequency side and becomes broader on increasing the temperature. The shift and broadening of

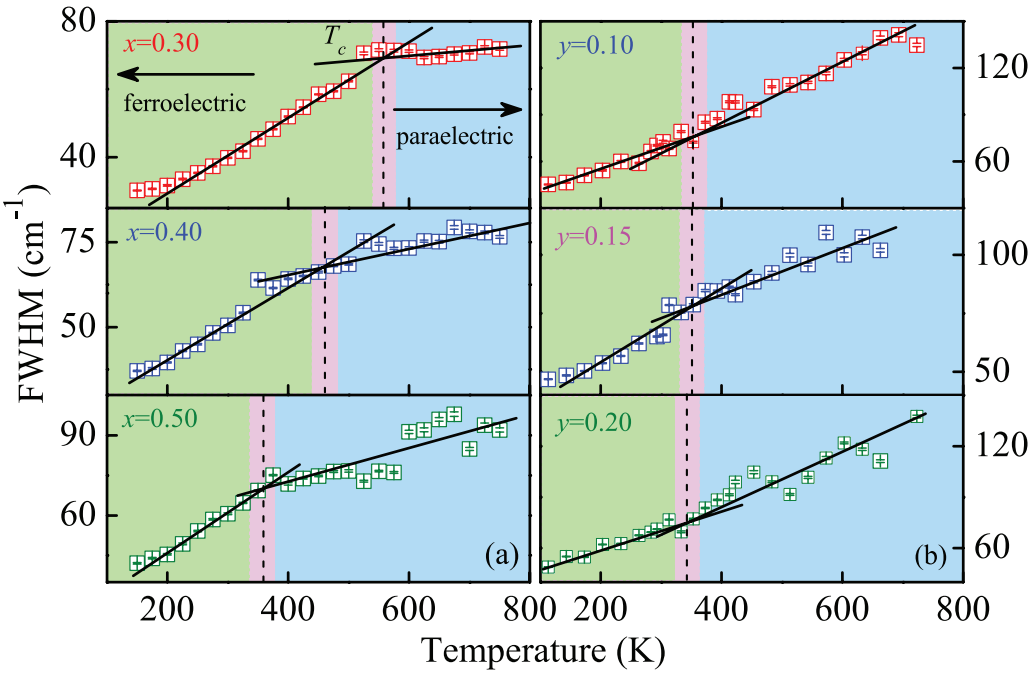

Figure 4. FWHM of the main mode (located at around 640 cm^{-1}) as a function of temperature for (a) SBN ceramics with a different Sr composition and (b) CSBN ceramics with a different Ca composition. The solid lines are applied as a guide for the eyes.

the two Raman bands result from many factors, such as the lattice disorder and a deformation potential interaction term. This may be associated with a change of structure with temperature and different Sr/Ba ratio [25, 32]. In addition, no soft mode was evidenced. The absence of an optical soft mode in SBN confirms the order–disorder type of ferroelectric phase transition [14].

To further discern the phase transition temperature of SBN ceramics and the effects of doping on its optical properties, the temperature evolution of full width at half maximum (FWHM) for different stoichiometries is discussed in detail. It can be seen from figure 4 that the band at about 640 cm^{-1} broadens linearly with temperature and the slope is modified in the paraelectric phase. For example, the temperature coefficient of SBN ($x = 0.3$) is about 0.11 cm^{-1} K^{-1} below 560 K and is 1.69×10^{-2} cm^{-1} K^{-1} above 560 K. It is believed that a moderation of the slope can help to define the T_c [25, 33]. The intersection of two straight lines gives us a relatively accurate phase transition temperature, which is 556 K for SBN ($x = 0.3$), 460 K for SBN ($x = 0.4$) and 359 K for SBN ($x = 0.5$). This can be well expressed by $T_c(x) = 860 - 1000x$. The result indicates that the parameter T_c decreases from about 556–360 K as the Sr composition increases from 0.3 to 0.5. The phenomenon can be attributed to the A site substitution that originated in the smaller ionic radius of Sr, as compared to the Ba element. The difference in the Ba–O and Sr–O bond distance and the presence of vacancies can lead to a large distortion of the octahedron. As for CSBN ceramics, however, the T_c changes slightly and almost remains unchanged at about 350 K, which is consistent with the results from the electrical method [22]. When the Ca^{2+} ions, whose ionic radius is smaller than Sr^{2+} and Ba^{2+}, are introduced into the SBN ceramics, it may move into the A2 site and substitute Sr^{2+} and Ba^{2+}. The appropriate substitution of smaller Ca^{2+} for Sr^{2+} and Ba^{2+} may enhance the structural distortion to some degree. However, it was reported that an atom with smaller metal–oxygen distance could occupy the C site [19]. Generally, the C site is occupied by oxygen atoms. Similar to the atoms in the A1 and A2 sites, a metal atom whose polarisation axis is in the z direction could occupy the C site. Thus, except for a few Ca^{2+} ions which move into A2 cite, most of the Ca^{2+} ions occupy the C site. The trigonal prism structure of the C site is somewhat locally symmetric and the vibration of the C site atoms do not contribute to Δz, where Δz is defined as the displacement developed by the metal atom along the polar direction. A simple experimental relationship between atomic displacement and the macroscopic ferroelectric properties of the Curie temperature was first reported by Abrahams *et al* [35]. The relationship of Δz and T_c for tungsten bronze-type displacive ferroelectrics is given by: $T_c = (2 \pm 0.09) \times 10^4 (\Delta z)^2$. Therefore, the introduction of Ca^{2+} slightly influences the T_c.

Note that the SBN ceramics are relaxor-type ferroelectric materials, whose relaxor degree is strongly dependent on the Sr composition [22]. We find that the slopes of the two straight lines approach each other with an increasing Sr fraction in figure 4(a). For low Sr composition ($x = 0.3$), SBN behaves like a normal ferroelectric material, which shows the well-defined peak in the dielectric constant. Moreover, increasing the Sr composition enhances its relaxor character, which show up as a diffuse phase transition (DPT) [22]. Thus, the T_c decreasing in SBN ceramics may be ascribed to the enhanced relaxor behaviour, which is owing to more Sr ions in the open TTB crystal structure. On the other hand, the SBN single crystals have a higher T_c than that of ceramics with the same composition [25]. The decrease of T_c of the SBN ceramics may

Table 1. Dielectric function parameters of the Tauc–Lorentz oscillator models for SBN and CSBN ceramics are extracted from the simulation of ellipsometric spectra.

Samples	$x = 0.3$, $y = 0$		$x = 0.4$, $y = 0$		$x = 0.5$, $y = 0$		$x = 0.5$, $y = 0.1$		$x = 0.5$, $y = 0.15$		$x = 0.5$, $y = 0.2$	
Temperature (K)	200	600	200	600	200	600	200	600	200	600	200	600
A (eV)	579	262	445	254	804	289	840	254	915	287	900	265
	(73)	(22)	(45)	(20)	(150)	(26)	(142)	(21)	(207)	(23)	(165)	(21)
C (eV)	1.31	2.23	1.44	2.21	1.11	2.32	0.92	2.24	1.06	2.18	1.11	2.19
	(0.1)	(0.1)	(0.1)	(0.1)	(0.1)	(0.1)	(0.1)	(0.1)	(0.1)	(0.1)	(0.1)	(0.1)
E_n (eV)	4.38	4.40	4.40	4.36	4.38	4.32	4.44	4.38	4.34	4.34	4.32	4.37
	(0.1)	(0.1)	(0.1)	(0.1)	(0.1)	(0.1)	(0.1)	(0.1)	(0.1)	(0.1)	(0.1)	(0.1)
E_t (eV)	4.08	3.60	3.99	3.60	4.16	3.63	4.18	3.57	4.19	3.63	4.17	3.59
	(0.1)	(0.1)	(0.1)	(0.1)	(0.1)	(0.1)	(0.1)	(0.1)	(0.1)	(0.1)	(0.1)	(0.1)
ε_∞	2.00	2.18	2.20	2.29	1.60	2.17	1.76	2.34	1.68	2.27	1.60	2.31
	(0.1)	(0.1)	(0.1)	(0.1)	(0.1)	(0.1)	(0.1)	(0.1)	(0.2)	(0.1)	(0.1)	(0.1)

Note: Note that the error bars are presented in brackets.

be attributed to the enhanced polar disorder in ceramics. The large amounts of grain boundaries in ceramics promote the formation of short range ordered polar nanoregions, which decrease the ferroelectric ordering temperature. Meanwhile, the relaxor behaviour of the CSBN ceramics is further enhanced with increased Ca content [27]. Thus, it becomes difficult to distinguish the slope modification of FWHM for CSBN. The considerable broadening of the phase transition may be related to the enhanced disorder and fluctuations, which is because smaller Ca^{2+} substitutes Sr^{2+} and Ba^{2+} at the A2 site, and Ca^{2+} moves into the C site [27].

The dielectric functions $[\tilde{\varepsilon}(E) = \varepsilon_1(E) + i\varepsilon_2(E)]$ and other significant parameters are extracted from the ellipsometric spectra as a supplement to investigate the phase transformation of SBN ceramics. In the present work, a three-layer model (air/surface roughness/ceramic) was used to evaluate the complex dielectric functions of SBN ceramics and the thickness of a rough layer. This layer was modelled by the Brüggeman effective-medium approximation (EMA) with a mixture of the bulk material (50%) and voids (50%). A single Tauc–Lorentz (TL) oscillator was applied to obtain the electronic band structure parameters of the SBN ceramics. The expression of the TL model is given by $\varepsilon_1(E) = \varepsilon_\infty + \frac{2}{\pi} P \int_{E_t}^{\infty} \frac{\xi\varepsilon_2(\xi)}{\xi^2 - E^2} d\xi$; $\varepsilon_2(E) = \frac{AE_nC(E-E_t)^2}{(E^2-E_n^2)^2 + C^2E^2} \frac{1}{E}$, $(E \geqslant E_t)$ and $\varepsilon_2(E) = 0$, $(E < E_t)$, where P is the Cauchy principal part of the integral, ε_∞ is the high frequency dielectric constant and E is the incident photon energy [36]. Meanwhile, A, C, E_n and E_t are the amplitude, broadening term, peak transition energy and Tauc gap energy of the oscillator, respectively. The above TL model follows the Kramers–Krönig transformation (KKT), which has been applied in ferroelectric ceramics or films successfully [37, 38]. All the values of the parameters for the fitted spectra obtained at 200/600 K are listed in table 1. The fitting procedure was carried out with a WVASE32 software package (Woollam Co, Inc). The best fitting pseudo-dielectric functions for SBN ($x = 0.3$) at 240 K and CSBN ($y = 0.2$) at 540 K are shown in figures 5(a) and (b). It should be emphasised that the thickness of the roughness layer can be fitted to about 8 nm for all the samples. So the scattering effects from the surface roughness layer can be neglected while comparing with the incident light spot of about 1 mm in diameter. The real part ε_1 and imaginary part ε_2 of dielectric functions for SBN ($x = 0.3$, and 0.5) and CSBN ($y = 0.1$, and $y = 0.2$) ceramics at several temperatures between 1.5 and 6.0 eV are plotted in figures 5(c)–(f). We find that the imaginary part ε_2 almost equals zero below 4.3 eV (near the absorption edge) and then increases sharply on increasing the phonon energy due to a strong optical absorption. On further increasing the temperature, ε_2 reaches the maximum at about 5 eV. The sharpening variation of the dielectric function observed could be intrinsically due to the temperature effects. We can also discern that the ε of all the ceramics shows a red-shift on increasing the temperature, which has an obvious effect on the dielectric functions. For example, the absorption edge of SBN ($x = 0.5$) decreases from 4.16 eV at 200 K–3.63 eV at 600 K. This could be attributed to the thermal expansion of the lattice and the enhanced distortion of the NbO_6 octahedra. It should be emphasised that the imaginary part of dielectric function $\varepsilon_2(E)$ of oxygen-octahedra ABO_3-type ferroelectrics are composed mostly of two main absorption bands located in the phonon energy ranges of 4–6 eV and 8–10 eV, which was previously reported by DiDomenico [39]. The fundamental significance of the BO_6 octahedra in the formation of band structure of ABO_3 ceramics was afterwards confirmed experimentally [37, 40]. The first-principles calculations on the electronic structures of $LiNbO_3$ [41], which possesses similar octahedra NbO_6 groups as in SBN, suggests that SBN is a displacive-type FE transition-metal oxide. The NbO_6 octahedron defines the lowest limit of the conduction band and the upper valence band. The valence bands (VBs) are primarily constituted of the O 2*p* states, whereas the conduction band (CB) originates mainly from Nb 4*d* states mixed with A-site transition metal (Sr 4*p*) states [42]. This indicates that the conduction band and valence band edges may change during the PE–FE transition, which reveals that the structure variation could influence the electronic structures.

In addition, a three-dimensional diagram of Tauc gap energy (E_t) with a function of temperature for the SBN ($x = 0.4$ and $x = 0.5$) and CSBN ($y = 0.1$,$y = 0.15$ and

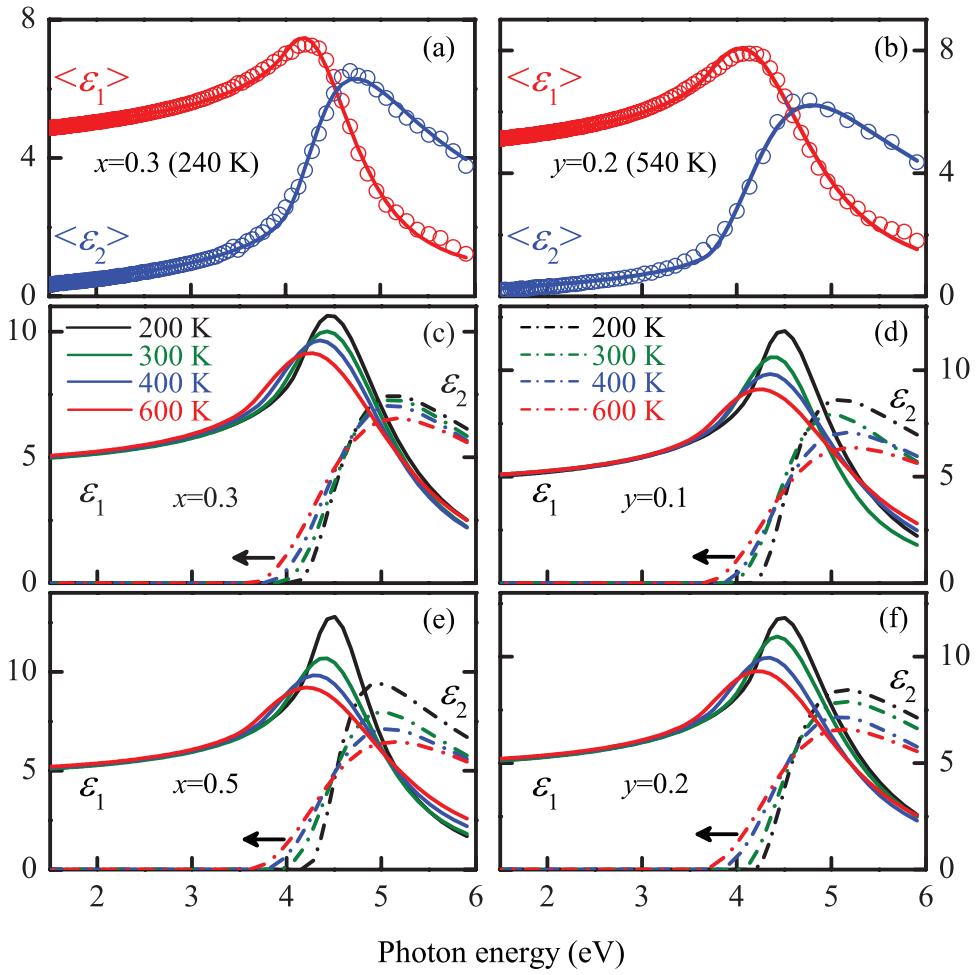

Figure 5. (a)–(b) The experimental (dots) and best fitting curves (solid lines) of the pseudo-dielectric functions of SBN ($x = 0.3$) ceramics at 240 K and CSBN ($y = 0.5$) ceramics at 540 K. Note that $< \varepsilon_i >$ is the dielectric function ε_i with the rough layer (50% bulk material and 50% voids) considered. (c)–(f) Real (ε_1) and imaginary (ε_2) parts of dielectric functions for SBN ($x = 0.3$, and $x = 0.5$) and CSBN ($y = 0.1$, and $y = 0.2$) ceramics measured at 200, 300, 400 and 600 K, respectively.

$y = 0.2$) ceramics are plotted in figure 6. Note that the E_t variation of SBN ($x = 0.3$) is not given because the phase transition temperature of SBN ($x = 0.3$) (about 556 K) is too close to the experiment's temperature upper limit (600 K) and it is hard to distinguish the variation of E_t. We find that the Tauc gap energy of all the samples shows a red-shift on increasing the temperature. Variations of E_t can be separated into three parts: the ferroelectric rhombohedral phase, the relaxation phase transformation range and the paraelectric tetragonal phase. Each part was linearly fitted and the temperature coefficient (dE_t/dT) of E_t differs for the three sections. Taking CSBN ($y = 0.1$) as an example, the slope of the fitted line for E_g is about 6.42×10^{-4} eV K^{-1} in the low temperature region and 2.97×10^{-3} eV K^{-1} in the intermediate temperature range, while the slope is estimated to be 8.90×10^{-4} eV K^{-1} in the high temperature part. The coefficients of the low and high temperature part are caused by temperature effects. Meanwhile, the intermediate coefficient can be interpreted by the phase change from the ferroelectric to the paraelectric phase due to the diffuse transition characteristics. It was reported that on increasing the Sr/Ba ratio a transformation from ferroelectric to relaxor behaviour takes

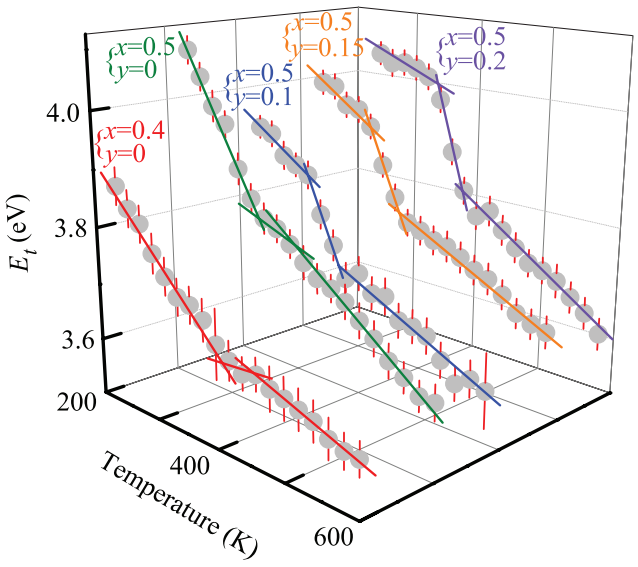

Figure 6. A three-dimensional comparison chart of the Tauc gap energy (E_t) varies with the temperature for SBN and CSBN ceramics. Note that the intermediate lines suggest the FE–PE transition temperature range.

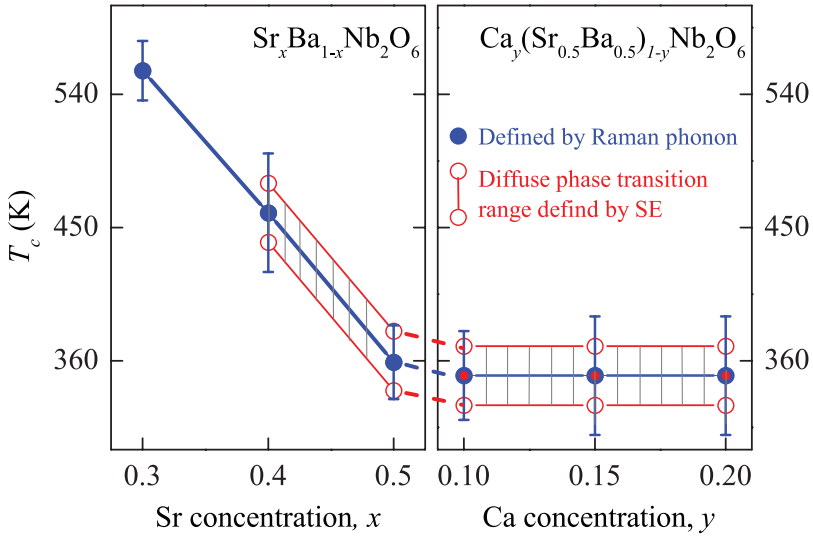

Figure 7. Curie temperature as a function of the stoichiometric composition x and y. The filled circle represents T_c obtained by Raman scattering and area labelled with the vertical lines between the circle is the phase transition temperature range derived by spectroscopic ellipsometry.

place [8]. As discussed in the Raman scattering above, the ionic radius of Sr^{2+} is smaller than Ba^{2+}. The substitution of Ba^{2+} by Sr^{2+} can lead to the modulation of stress and a rearrangement of the structural framework, which will affect the electronic band structures. For further validation of the phase transition temperature investigated by SE measurement, we compare T_c obtained by both methods in figure 7. The Curie temperature obtained by Raman scattering lies exactly in the diffuse transition temperature range obtained by SE. Indeed, good agreement between both kinds of measurements is obtained, corroborating the validity of spectroscopic ellipsometry for measuring the Curie temperature of SBN ceramics. These results indicate that SE could be a possible method to identify the phase transition of relaxor ferroelectric materials.

4. Conclusions

In summary, the lattice vibrational spectra of ferroelectric SBN ceramics can be affected by the variation of Sr/Ba ratios. The composition dependence of the phase transition temperature was investigated using Raman spectroscopy in the temperature range of 150–750 K, and spectroscopic ellipsometry in the photon energy range of 1.5–6 eV. On increasing the temperature, the V_3 modes located about 640 cm^{-1} become softer and broader. It is clear that increasing the Sr composition (from 0.30 to 0.50) leads to the shrinking of T_c (from 556 to 359 K). Meanwhile, the Ca dopant makes the V_3 modes softer and the phase transition become more diffuse. Furthermore, the relaxor behaviour and Curie temperature could be well elucidated by SE measurements. The results obtained from the combination of Raman scattering and spectroscopic ellipsometry give us a comprehensive understanding of the phase transformation of SBN ceramics.

Acknowledgments

This work was financially supported by Major State Basic Research Development Program of China (Grant Nos. 2013CB922300 and 2011CB922200), the Natural Science Foundation of China (Grant Nos. 11374097 and 61376129), the Projects of Science and Technology Commission of Shanghai Municipality (Grant Nos. 15JC1401600, 14XD1401500, 13JC1402100 and 13JC1404200), and the Program for Professor of Special Appointment (Eastern Scholar) at the Shanghai Institutions of Higher Learning.

References

[1] Viehland D, Li J F and Colla E V 2004 *J. Appl. Phys.* **96** 3379
[2] Noheda B, Cox D E and Shirane G 2002 *Phys. Rev.* B **66** 054104
[3] Randall C A, Bhalla A S, Shrout T R and Cross L E 1990 *J. Mater. Res.* **5** 829
[4] Ma C, Guo H Z and Tan X L 2013 *Adv. Funct. Mater.* **23** 5261
[5] Jones G O and Thomas P A 2002 *Acta Cryst.* B **58** 168
[6] Baker D W, Thomas P A, Zhang N and Glazer A M 2009 *Appl. Phys. Lett.* **95** 091903
[7] Baker D W, Thomas P A, Zhang N and Glazer A M 2009 *Acta Cryst.* B **65** 22
[8] Shvartsman V V and Kleemann W 2008 *Phys. Rev.* B **77** 054105
[9] Tian L, Scrymgeour D A, Sharan A and Gopalan V 2003 *Appl. Phys. Lett.* **83** 21
[10] Hamad M A 2012 *Appl. Phys. Lett.* **100** 192908
[11] Dul'kin E, Kojima S and Roth M 2012 *J. Appl. Phys.* **111** 084101
[12] Molina P, Ramírez M D L O and Bausá L E 2008 *Adv. Funct. Mater.* **18** 709
[13] Kleemann W, Dec J, Shvartsman V V, Kutnjak Z and Braun T 2006 *Phys. Rev. Lett.* **97** 065702
[14] Buixaderas E, Gregora I, Hlinka J, Dec J and łukasiewicz T 2012 *Phase Transit.* **86** 217

[15] Glass A M 1968 *Appl. Phys. Lett.* **13** 147
[16] Glass A M 1969 *J. Appl. Phys.* **40** 4699
[17] Wilde R E 1991 *J. Raman Spectrosc.* **22** 321
[18] Trubelja M P, Ryba E and Smith D K 1996 *J. Mater. Sci.* **31** 1435
[19] Jamieson P B, Abrahams S C and Bernstein J L 1968 *J. Chem. Phys.* **48** 5048
[20] Pandey C S, Schreuer J, Burianek M and Muhlberg M 2013 *Appl. Phys. Lett.* **102** 022903
[21] Faria J L B, Freire P T C, Ayala A P, Melo F E A, Filho J M, Paschoal C W A, Santos I A and Eiras J A 2003 *J. Raman Spectrosc.* **34** 826
[22] Zhang J, Wang G S, Gao F, Mao C L, Cao F and Dong X L 2013 *Ceram. Int.* **39** 1971
[23] Chen X, Hu Z G, Duan Z H, Chen X F, Wang G S, Dong X L and Chu J H 2013 *J. Appl. Phys.* **114** 043507
[24] Jiang K, Li W W, Chen X G, Zhan Z N, Sun L, Hu Z G and Chu J H 2012 *J. Raman Spectrosc.* **43** 583
[25] Speghini A, Bettinelli M, Caldiño U, Ramírez M O, Jaque D, Bausá L E and Solé J G 2006 *J. Phys. D: Appl. Phys.* **39** 4930
[26] Yao Y B, Liu W C, Mak C L and Wong K H 2011 *AIP Adv.* **1** 032172
[27] Zhang J, Dong X L, Cao F, Guo S B and Wang G S 2013 *Appl. Phys. Lett.* **102** 102908
[28] Venturini F L, Spencer E G, Lenzo P V and Ballmani A A 1968 *J. Appl. Phys.* **39** 343
[29] Woike T, Granzow T, Dörfler U, Poetsch C, Wöhlecke M and Pankrath R 2001 *Phys. Status Solidi* A **186** R13
[30] David C, Tunyagi A, Betzler K and Wöhlecke M 2007 *Phys. Status Solidi* B **244** 2127
[31] Dorywalski K, Andriyevsky B, Cobet C, Piasecki M, Kityk I V, Esser N, łukasiewicz T and patryn A 2013 *Opt. Mater.* **35** 887
[32] Samanta K, Arora A K, Ravindran T R, Ganesamoorthy S, Kitamura K and Takekawa S 2012 *Vib. Spectrosc.* **62** 273
[33] Kasprowicz D, Runka T, Speghini A, Falcomer D, García J and Bettinelli M 2008 *J. Lumin.* **128** 985
[34] Kasprowicz D, Lapinski A, Runka T, Speghini A and Bettinelli M 2009 *J. Alloy Compd.* **478** 30
[35] Abrahams S C, Kurtz S K and Jamieson P B 1968 *Phys. Rev.* **172** 551
[36] Jellison J G E and Modine F A 1996 *Appl. Phys. Lett.* **69** 371
Jellison J G E and Modine F A 1996 *Appl. Phys. Lett.* **69** 2137
[37] Duan Z H, Jiang K, Xu L P, Li Y W, Hu Z G and Chu J H 2014 *J. Appl. Phys.* **115** 054107
[38] Zhang S, Zhang J Z, Han M J, Li Y W, Hu Z G and Chu J H 2014 *Appl. Phys. Lett.* **104** 041106
[39] DiDomenico M and Wemple S H 1969 *J. Appl. Phys.* **40** 720
[40] Andriyevsky B, Dorywalski K, Kityk I, Piasecki M, łukasiewicz T, Świrkowicz M, Patryn A, Dec J, Esser N and Cobet C 2011 *Ferroelectrics* **417** 14
[41] Ching W Y, Gu Z-Q and Xu Y-N 1994 *Phys. Rev.* B **50** 3
[42] Mamedov A M 1982 *Ferroelectrics* **45** 55